How Predictability Depends on the Nature of Uncertainty in Initial Conditions in a Coupled Model of ENSO

YUN FAN* AND M. R. ALLEN

Atmospheric, Oceanic, and Planetary Physics, Department of Physics, University of Oxford, Oxford, and Space Science Department, Rutherford Appleton Laboratory, Oxfordshire, United Kingdom

D. L. T. ANDERSON

Atmospheric, Oceanic, and Planetary Physics, Department of Physics, University of Oxford, Oxford, and ECMWF, Reading, United Kingdom

M. A. BALMASEDA

ECMWF, Reading, United Kingdom

(Manuscript received 1 February 1999, in final form 3 December 1999)

ABSTRACT

The predictability of any complex, inhomogeneous system depends critically on the definition of analysis and forecast errors. A simple and efficient singular vector analysis is used to study the predictability of a coupled model of El Niño–Southern Oscillation (ENSO). Error growth is found to depend critically on the desired properties of the forecast errors (''where and what one wants to predict''), as well as on the properties of the analysis error (''what information is available for that prediction'') and choice of optimization time. The time evolution of singular values and singular vectors shows that the predictability of the coupled model is clearly related to the seasonal cycle and to the phase of ENSO. It is found that the use of an approximation to the analysis error covariance to define the relative importance of errors in different variables gives very different results to the more frequently used ''energy norm,'' and indicates a much larger role for sea surface temperature information in seasonal (3–6-month timescale) predictability. Seasonal variations in the predictability of the coupled model are also investigated, addressing in particular the question of whether seasonal variations in the dominant singular values (the ''spring predictability barrier'') may be largely due to the seasonality in the variance of SST anomalies.

1. Introduction

A very important component of any prediction system is the ability to understand the evolution of forecast skill. In a chaotic system, the fastest growing singular vectors (Lorenz 1965; Palmer 1996; Moore and Kleeman 1996) may dominate the forecast error growth. Since initial errors are inevitable, the optimal error growth, measured in the linear regime by the first singular value, gives an upper limit on predictability. Even if initial errors are large enough to evolve into a nonlinear regime, or model errors are significant, then the fastest growing singular vectors are still of interest as a practical tool for the initialization of ensemble forecasts.

There has been a range of applications of the singular vectors to El Niño–Southern Oscillation (ENSO). Blumenthal (1991) used a statistical reduction model that is a best fit to the output of the full Zebiak and Cane model (ZC; 1987) to study the growth of initial error in the ZC model. He found that there is one growing singular vector with largest growth in the spring. The final pattern of the optimal sea surface temperature (SST) perturbation is very similar to the model ENSO pattern. A similar method has been used by Xue et al. (1994). The results are similar in some aspects to those in Blumenthal (1991) in that the structure of the fastest growing singular vector at the initial and final time does not change much with the seasons at which the forecast is initialized.

Moore and Kleeman (1996) used an intermediate coupled model of ENSO to construct a tangent linear model

* Current affiliation: Center for Ocean–Land–Atmosphere Studies, Institute of Global Environment and Society, Calverton Maryland.

Corresponding author address: Dr. Yun Fan, Center for Ocean–Land–Atmosphere Studies, 4041 Powder Mill Road, Suite 302, Calverton, MD 20705.
E-mail: fan@cola.iges.org

and its adjoint, and computed the corresponding singular vectors. They obtained somewhat different initial error patterns that started from the western Pacific with a deepened thermocline, a relatively ''noisy'' SST and wind field, and then moved to the central Pacific and amplified through penetrative convection.

Chen et al. (1997) used the Battisti (1988) version of the ZC model and applied an approximate method to obtain the linear propagator directly from the full coupled model, and then calculated singular vectors maximizing only SST variance subject to an initial perturbation in the SST field. They found one dominant singular vector that is not sensitive to the initial time in the annual cycle nor to the optimization time. The initial (optimal perturbation) pattern consists of an east–west dipole in the entire tropical Pacific basin superimposed on a north–south dipole in the eastern tropical Pacific. The final pattern resembles the model ENSO mode. However, the magnitude of possible error growth is highly dependent on the phase of the seasonal cycle and the phase of the ENSO cycle at which the perturbation is applied.

Xue et al. (1997a,b) used the ZC model from which a linear tangent model is constructed using the method suggested by Lorenz (1965) based on empirical orthogonal function (EOF) perturbation. Their results are similar in some aspects to these of Chen et al. (1997). However, there are some differences in the singular vector growth rate and variability of the optimal final patterns. Thompson (1998) also studied the properties of the optimal growth structure for a linearized version of the Battisti (1988) coupled model of ENSO and found that in some aspects the singular vectors and their growth rates were in good agreement with those produced in Chen et al. (1997) and Xue et al. (1997a).

Penland and Sardeshmukh (1995), using a linear stochastic ENSO model derived from observations, found only one growing singular vector. This singular vector is somewhat similar to that from Chen et al. (1997) in the large scale, but it also shows some differences, such as a negative anomaly in the optimal initial SST pattern in the central tropical Pacific, a band of positive anomaly in the Northern Hemisphere subtropics, and a similar feature in the Southern Hemisphere.

A point that is not made very explicit in previous work is that the definition of predictability in any dynamical system is not unique, since it depends on the measure of error, that is, the choice of error norm. For example, minimizing prediction error in different geographical locations may require different initial information and therefore be subject to different levels of predictability. Likewise, initial errors in different locations and different variables may be amplified by different physical processes. Thus, understanding these aspects of the predictability of the system has considerable practical importance. In this paper, we will focus on the following questions. 1) How does the predictability of the forecast system depend on the variables we want to predict and on their geographical location? 2) To predict these variables, what initial information is required and how does predictability depend on its distribution? 3) How can we compare the relative importance of different error growth processes in the coupled model?

This article is organized as follows. The coupled model and an efficient method of calculating approximate singular vectors are described in section 2. In section 3, we examine how the predictability of SST depends on the geographical distribution of accepted forecast error under some idealized analysis errors. Then, in section 4, various ''multivariable'' norms, involving both SST and subsurface information, are used to investigate different error growth processes. In section 5, the variability of the singular vectors and singular values over the 1970s and 1980s is investigated, and the relative importance of different error growth processes and the seasonality of singular values are further explored. Conclusions are discussed in section 6.

2. The coupled model and analysis method

a. The forecast system

The coupled model used here is one of a hybrid nature, consisting of a dynamical ocean coupled to a statistical atmosphere (Balmaseda et al. 1994). The ocean model is derived from that described in Anderson and McCreary (1985) and McCreary and Anderson (1991), but extended to two active layers. Dynamics are based on the shallow-water equations on the equatorial β plane. The model includes explicit nonlinear thermodynamics for both layers, accounting for horizontal advection, vertical heat transport, diffusion, and, in the first layer, wind stress and surface heat flux, but no freshwater flux.

The surface heat flux was derived from Oberhuber (1988) plus two additional terms: a constant correction term ($Q_{0\mathrm{mod}}$) that ensures the model is in equilibrium with the forcing, and a relaxation term to prescribed monthly climatological SST ($T_{0\mathrm{mod}}$) taken to be the SST of the model equilibrium:

$$Q_s = Q_{\mathrm{Oberhuber}} + Q_{0\mathrm{mod}} + \lambda(T - T_{0\mathrm{mod}}). \qquad (1)$$

To create the initial conditions, the ocean model is forced by observed wind stress [based on data from The Florida State University (FSU), Goldenberg and O'Brien 1981] during the period 1961–91 (control run). The wind forcing is therefore the only information about the state of the real world that is used to initialize forecasts, since the observed SST anomalies do not intervene in the formulation of the heat flux. The fact that we do not use SST or **H** information to initialize the model simplifies the discusion of analysis error as discussed in section 4b.

The control simulation is also used to derive the empirical atmosphere, which is a statistically derived anomaly model. It is based on the assumption that near-

surface wind stress anomalies (relative to the monthly mean climatology) are a linear response to some function of the model SST. The output of control simulation is used to find the regression coefficients between the wind stress anomalies and the first six principal components of the model SST anomalies, with seasonal variation. The details of the formulation can be found in Balmaseda et al. 1994.

b. Definition of the errors

Let the vector $\mathbf{x}$ represent the state variables of the coupled model that is governed by the following equation:

$$\mathbf{x}(t + \delta t) = \mathcal{M}[\mathbf{x}(t)], \tag{2}$$

where $\mathcal{M}$ is a nonlinear operator. If $\mathbf{x}'$ is a perturbation of $\mathbf{x}$, then

$$\mathbf{x}'(t + \delta t) = \mathcal{M}[\mathbf{x}(t) + \mathbf{x}'(t)] - \mathcal{M}[\mathbf{x}(t)]. \tag{3}$$

In the linear regime, we can write the above equation as follows:

$$\mathbf{f} = \mathbf{L}\mathbf{g}, \tag{4}$$

where $\mathbf{L}$ is a linearized version of $\mathcal{M}$, called the linear propagator, and $\mathbf{g}$ and $\mathbf{f}$ are initial and final error vectors, $\mathbf{x}'(t)$ and $\mathbf{x}'(t + \delta t)$, respectively.

In order to measure error growth, we require a scalar definition of the ''size'' of the error at both forecast initialization and target times. In the simplest case of uncorrelated errors, these are most conveniently defined in terms of weighted sums of squares, $\Sigma_i w_{Ai} g_i^2$ and $\Sigma_i w_{Fi} f_i^2$. More generally, initial and final errors can be defined by the quadratic forms, $\mathbf{g}^{\mathrm{T}}\mathbf{W}_A\mathbf{g}$ and $\mathbf{f}^{\mathrm{T}}\mathbf{W}_F\mathbf{f}$, where the $\mathbf{W}$ are simply matrices of weights, still to be defined, otherwise known as the ''error metrics'' or ''norms.'' Since our focus in this paper is the definition of error, it is important to recognize that there are situations which would not be well represented by such quadratic forms, despite their apparent generality. For example, if the crucial question was whether or not the forecast quantity would exceed a certain value (e.g., in a flood prediction problem), then a quadratic form would not be an ideal measure of uncertainty, since it assigns equal weight to both positive and negative errors. For consistency with the bulk of the literature on error growth, however, we confine attention to the quadratic definition.

There are two approaches to interpreting $\mathbf{W}_F$ and $\mathbf{W}_A$. The first is to define them in terms of a physically interpretable scalar quantity, such as the total energy or enstrophy of a perturbation; this is most informative in studies focusing on mechanisms of error growth. The second is to define them in terms of the actual errors that are likely to occur in a forecast based on this particular model; we focus on this second approach, which (by definition) has greater relevance to the practical ensemble forecasting situation.

The interpretation of the forecast norm, $\mathbf{W}_F$, is straightforward; weights should be large in regions where we desire a good forecast, so a natural choice would be for $\mathbf{W}_F$ to be the inverse of the target forecast error covariance. There is no reason in principle why $\mathbf{W}_F$ should equal $\mathbf{W}_A$ but interpretation of error growth factors (the singular values) becomes quite subjective in the case that it does not (e.g., doubling the elements of $\mathbf{W}_F$ without changing $\mathbf{W}_A$ would double all singular values). Because we are not attempting practical forecasts in this study, we are at liberty to set $\mathbf{W}_F$ to be whatever we like, so for simplicity, we will set $\mathbf{W}_F = \mathbf{W}_A$ throughout, except in the case of forecasts focusing on specific regions.

In this practical approach, the analysis norm, $\mathbf{W}_A$, should reflect how forecasts are initialized. In an ensemble forecast system, isotropic random perturbations (i.e., with equal variance in all components) are weighted by the estimated analysis error to give ''realistic'' initial perturbations. For consistency, we require $\mathbf{W}_A$ to be chosen such that two perturbations of equal size are equally likely to be generated by the ensemble initialization procedure. This requires $\mathbf{W}_A$ to be the inverse of the estimated analysis error covariance, or $\mathbf{W}_A = \mathbf{C}_A^{-1}$. The reason is as follows: if $\mathbf{g}$ is a vector of typical analysis errors, then, by definition,

$$\boldsymbol{\varepsilon}(\mathbf{g}\mathbf{g}^{\mathrm{T}}) \equiv \mathbf{C}_A \quad \text{and} \quad \boldsymbol{\varepsilon}(\mathbf{g}^{\mathrm{T}}\mathbf{C}_A^{-1}\mathbf{g}) = 1, \tag{5}$$

where $\boldsymbol{\varepsilon}$ is the expectation operator. Thus any two equally probably analysis errors would be given equal weight under this analysis norm. A method of estimating $\mathbf{C}_A^{-1}$ from the simulated analysis error covariance matrix is given in appendix B.

If the forecast initialization system is consistent and the model can be treated as perfect, we require $\mathbf{C}_A$ to approximate the actual analysis error covariance. The characteristics of the analysis error are often very poorly known. They depend both on the observing system used to initialize the model (large errors in data-sparse regions) and also, in a highly inhomogenous system, on the dynamics of the system itself. In the case of the tropical Pacific, for example, the strongest variability occurs in the equatorial waveguide region, so we should expect large analysis errors in this region even though it is relatively well observed by the Tropical Ocean and Global Atmosphere–Tropical Atmosphere–Ocean (TOGA–TAO) buoy array.

In the case of an imperfect model, the quantity of interest is not the analysis error itself, since if we were to initialize such a model with a complete and accurate set of observations of the true system (supposing this were available) it would fail to generate a sensible forecast because of model error. Rather, $\mathbf{C}_A$ should reflect the statistics of the difference between the analysis used to initialize the forecast and the unknown ''shadowing trajectory'' (Gilmour 1999) that provides the most accurate forecast possible with this imperfect model. For simplicity, we will focus our discussion on the perfect-

model scenario, but it is worth noting that in the case of an imperfect model, the dynamics of the model itself play an even greater role in determining the appropriate analysis error covariance: if a model is only capable of displaying variability on large spatial scales, for example, then these scales must dominate the difference between the analysis and shadowing trajectories even if the real world displays more small-scale variability.

In almost all situations, $\mathbf{W}_F$ and $\mathbf{W}_A$ will be real symmetric, so they can be expressed in terms of the Cholesy decomposition:

$$\mathbf{W}_A = \mathbf{P}_A^{\mathrm{T}}\mathbf{P}_A \text{ and } \mathbf{W}_F = \mathbf{P}_F^{\mathrm{T}}\mathbf{P}_F. \tag{6}$$

The projection operators, $\mathbf{P}_F$ and $\mathbf{P}_A$, yield weighted vectors, $\tilde{\mathbf{f}} = \mathbf{P}_F\mathbf{f}$ and $\tilde{\mathbf{g}} = \mathbf{P}_A\mathbf{g}$, in which expected errors are isotropic (uncorrelated and equal variance across components). The ratio of final error to initial error can then be written

$$\lambda^2 = \frac{\tilde{\mathbf{f}}^{\mathrm{T}}\tilde{\mathbf{f}}}{\tilde{\mathbf{g}}^{\mathrm{T}}\tilde{\mathbf{g}}} = \frac{\mathbf{f}^{\mathrm{T}}\mathbf{P}_F^{\mathrm{T}}\mathbf{P}_F\mathbf{f}}{\mathbf{g}^{\mathrm{T}}\mathbf{P}_A^{\mathrm{T}}\mathbf{P}_A\mathbf{g}} = \frac{\mathbf{f}^{\mathrm{T}}\mathbf{W}_F\mathbf{f}}{\mathbf{g}^{\mathrm{T}}\mathbf{W}_A\mathbf{g}}. \tag{7}$$

Substituting for $\mathbf{f}$ using Eq. (4) gives

$$\lambda^2 = \frac{\tilde{\mathbf{g}}^{\mathrm{T}}\mathbf{P}_A^{-1\mathrm{T}}\mathbf{L}^{\mathrm{T}}\mathbf{P}_F^{\mathrm{T}}\mathbf{P}_F\mathbf{L}\mathbf{P}_A^{-1}\tilde{\mathbf{g}}}{\tilde{\mathbf{g}}^{\mathrm{T}}\tilde{\mathbf{g}}} = \frac{\tilde{\mathbf{g}}^{\mathrm{T}}\tilde{\mathbf{L}}^{\mathrm{T}}\tilde{\mathbf{L}}\tilde{\mathbf{g}}}{\tilde{\mathbf{g}}^{\mathrm{T}}\tilde{\mathbf{g}}}, \tag{8}$$

where

$$\tilde{\mathbf{L}} = \mathbf{P}_F\mathbf{L}\mathbf{P}_A^{-1}, \tag{9}$$

provided that $\mathbf{P}_A^{-1}$ exists. If it does not, a pseudo inverse can be introduced to define an approximate error growth rate in a restricted space (see appendix B).

The vector $\tilde{\mathbf{g}}$ that maximizes λ^2 in Eq. (8) is the first eigenvector of $\tilde{\mathbf{L}}^{\mathrm{T}}\tilde{\mathbf{L}}$, and can be obained from a singular value decomposition (SVD) of $\tilde{\mathbf{L}}$. If $\mathbf{P}_A$ is nondiagonal, the elements of $\tilde{\mathbf{g}}$ will not correspond to spatial locations, so we visualize these singular vectors by examining $\mathbf{R}_A^{-1}\tilde{\mathbf{g}}$, where (in the simplest case of the rows of $\mathbf{P}_A$ being mutually uncorrelated, as in all the examples here) the rows of $\mathbf{R}_A$ are the rows of $\mathbf{P}_A$, normalized to unity (i.e., $\mathbf{R}_A$ corresponds to a pure rotation, while $\mathbf{P}_A$ corresponds to a rotation with weighting). Corresponding final error patterns are obtained similarly from the SVD.

c. Estimation of the linear propagator of the coupled model

Rather than constructing the full tangent linearization of the original model, we use an approximation suggested by Lorenz (1965), modified to obtain the linear propagator efficiently from the full coupled model. The details are given in appendix A, but the basic principle is to perturb the full coupled model using a small number (order 10–50) of patterns (forming an orthonormal set), which are assumed to span typical analysis errors. The choice of patterns is quite arbitrary, but should reflect accessible modes of variability of the model; by construction, the atmosphere model can only respond to large-scale patterns of SST anomalies, which restricts the scale of the growing coupled instabilities. We use EOFs derived from a control integration of the ocean model forced with observed wind stress to construct the linear propagator; these large-scale patterns are accessible to the model by construction and so should capture any likely error growth processes.

3. Error growth in SST

The simplest analysis is to examine error growth in one variable (e.g., SST) only, to give equal weight to all analysis errors ($\mathbf{W}_A = \mathbf{I}$) and to use simple geographical projection operators for $\mathbf{P}_F$. For example, we could prescribe $\mathbf{P}_F$ to be diagonal with unit entries for the area in which we are interested and zero elsewhere. In physical terms, this is equivalent to the question: to predict SST in a given region, where is the most important initial SST information located?

a. Predicting SST over the whole tropical Pacific

In predicting SST over the whole tropical Pacific, we assume that $\mathbf{P}_A$ and $\mathbf{P}_F$ are uniform diagonal matrices spanning the domain shown in Fig. 1. Both the initial and final singular vectors under this ''SST to SST'' (**TT**) norm are shown for 3- and 12-month optimization times. The striking similarity between both initial and final patterns indicates the limited number of error growth modes available to this model. At this time, and most others, only one or two singular values exceed unity. The main signals, located in the central–eastern equatorial Pacific, indicate that to predict future SST in the whole tropical Pacific for up to 12 months, the most important initial SST information is located in the central–eastern tropical Pacific. The figure shows the singular vectors for a forecast initialized in January 1982, but the patterns are similar when forecasts are initialized at other dates. The error growth rate, however, indicated by the singular values, is sensitive to the initialization time.

We can compare our results with those from recent papers using the SST norm. Chen et al. (1997) used the Battisti (1988) version of the Zebiak and Cane model (ZC) (1987), while Thompson (1998) used a linearized version of the Battisti model to repeat part of Chen's work. Their results show that the initial and final patterns of the singular vectors have large-scale structures with the main signals located in the central–eastern Pacific. The error growth rates vary with the seasonal cycle and ENSO phase and have values comparable to ours. Xue et al. (1997a) used the ZC model in a reduced EOF space (keeping 37 EOFs for the SST). The optimal initial pattern is characterized by north–south and west–east dipoles in optimal SST field. The final pattern shows a mature ENSO phase. Compared with Chen's results, the SST optimizations from Xue are more equa-

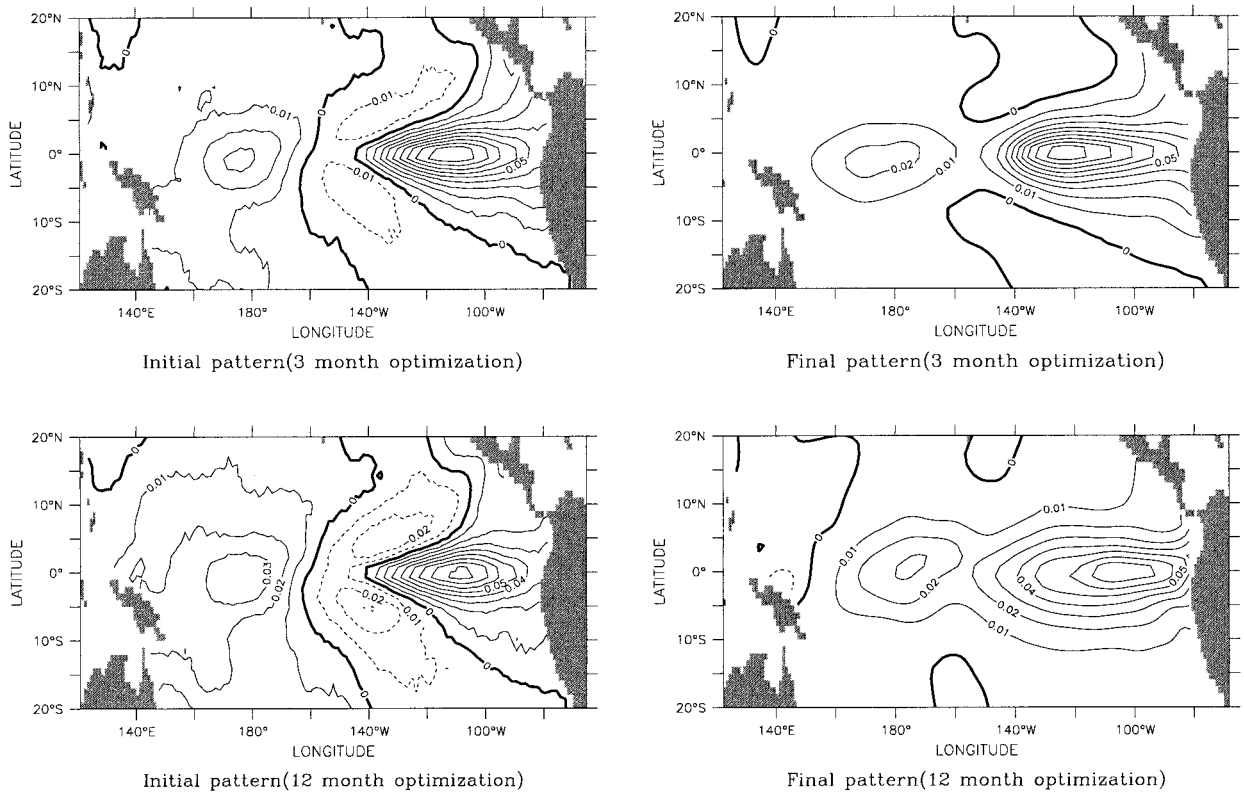

FIG. 1. First singular vectors for optimization times of 3 and 12 months, started in Jan 1982 under uniform SST to SST norm. The corresponding singular values are 1.6 and 3.7, respectively.

torially confined but have comparable optimal growth rates.

Moore and Kleeman (1996) use an intermediate coupled model to compute the singular vectors by constructing and using the model adjoint. They found that the singular vector spectrum is dominated by one member. The optimal final SST pattern is large scale, with its largest SST anomaly mainly located around 180°. In the case of SST norm, their optimal initial SST perturbation is a large-scale dipole pattern, with a strong negative anomaly in the western Pacific and a relatively weaker positive anomaly in the central–eastern Pacific (Moore and Kleeman 1997b).

Using the observed SSTs in the Indian and Pacific Oceans to build a linear Markov model, Penland and Sardeshmukh (1995) computed the SST structure of the dominant singular vectors under the SST norm. They also found only one growing singular vector. The main signal in the optimal initial patterns is located in the southeastern Pacific, which is more similar to those in Chen and Thompson's optimal initial SST patterns, while Xue and our optimal initial SST in the eastern Pacific seems more constrained to the equator. There is a optimal negative anomaly in Penland and Sardeshmukh's initial pattern in the central tropical Pacific, which is similar to those in our optimal initial SST patterns. There is an optimal positive anomaly in the western Pacific that is also found in our optimal initial SST patterns but not in Moore and Kleeman, Chen, Xue, and Thompson's results. The reason for other coupled models that cannot produce these negative and positive anomalies well in the central–western tropical Pacific, may be related to their atmospheric models, which cannot generate the correct remote wind stress response to the SST anomalies in the central–eastern Pacific, while the statistical atmosphere model can produce such a wind stress response.

Despite differences among the coupled models and the methods used to calculate the singular vectors, there is some agreement. The optimal initial and final patterns from many different models have large-scale features in the tropical Pacific. Most of the time, the error growth in the coupled models is controlled by one dominant growing pattern and its final pattern resembles the model ENSO mode. The error growth rates from all these results vary with the seasonal cycle and the phase of ENSO.

The differences in the singular vectors reflect different physics in different coupled models. Different versions of ZC model (used by Blumenthal 1991; Xue et al. 1994, 1997a; Chen et al. 1997; Thompson 1998) show that the most important signals are located in the eastern Pacific, where the models have the largest SST variability and wind stress mainly responds to local SST

anomalies. Thus, the atmosphere and ocean are closely coupled in the eastern Pacific. The results from Moore and Kleeman show that in their model, the coupling is dominant in the western and central tropical Pacific where the rapid error growth is associated with penetrative convection anomalies that only exist over regions where the SST ≥ 28°C. In their model, ocean and atmosphere are strongly coupled in the central–western tropical Pacific.

Our results also reflect the coupling physics in our model. Our model has the largest SST variability in the central–eastern Pacific and the statistical atmospheric model is constructed based on the statistical relationship between wind stress anomalies and SST anomalies along the whole tropical Pacific. The atmospheric model mainly responds to the SST anomalies in the central–eastern tropical Pacific and with the largest wind stress response located from near the date line to the central Pacific. There is also a response to SST anomalies in the western tropical Pacific, similar to the one found by Penland and Sardeshmukh.

Because of our use of a reduced-rank linear propagator $\tilde{\mathbf{L}}$ (see appendix A), initial error patterns are confined to the subspace spanned by the leading 10 EOFs of the control integration and are therefore constrained to represent large scales. However, increasing the rank to 50 had little impact on the shape of the patterns. Use of an exact model adjoint would allow smaller-scale error patterns to play a larger role but, as noted above in the discussion of the analysis error, we are only interested in error patterns that are accessible to a forced or coupled integration of this model. Given our initialization procedure (forcing with observed winds), very small-scale patterns would never feature in either the forced integration or the ideal shadowing trajectory of the coupled model, which provides a hypothetical best possible forecast in any particular situation. Small-scale errors can therefore consistently be ignored in this study, although they might play a larger role with a different initialization procedure, such as nudging toward observed subsurface ocean data. In any case, we would hestitate to draw conclusions from small-scale structures simulated by this model, since the dynamics of the model are unlikely to be realistic on any but the largest scales. This EOF-based analysis provides, therefore, a necessarily incomplete picture of possible errors but one which, we believe, encompasses the errors that can sensibly be studied with this kind of model.

b. Predicting SST in the tropical western Pacific

Compared to the eastern Pacific, SST variability in the tropical western Pacific is relatively small, and so, under uniform weighting, singular vectors for the entire Pacific will be dominated by what happens in the east; no matter what perturbation is applied, it will tend to have more impact on eastern Pacific than western Pacific SSTs simply because the former vary more easily. The real atmosphere, however, is much more sensitive to SST fluctuations of a given magnitude in the western Pacific (Palmer and Mansfield 1984). So it may be desirable to predict SST more accurately in the tropical western Pacific than in the east.

To examine this issue, we simply assign a weight of 1.0 to forecast errors in the western tropical Pacific and a weight of 0.0 to forecast errors in the eastern tropical Pacific. Initial errors remain uniformly weighted over the whole model domain. Results are shown in Fig. 2. Final singular vectors are confined to the west by construction, but examination of the initial singular vectors (left panel) indicates that, for this coupled system, the SST information needed to predict SST anomalies in the tropical western Pacific in three month's time is mainly located in the tropical western Pacific itself. To predict SST anomalies in the tropical western Pacific at a lead of one year, however, we need to pay most attention to initial SST information in the tropical eastern Pacific. At intervening lead times (6–9 months, not shown), SST information in both east and west is important.

The striking similarity between the initial patterns for 12-month optimization in Figs. 1 and 2, again may be explained by the limited number of instability mechanisms available; regardless of where one wants to predict SST, the same initial pattern is important if the lead time is sufficiently long.

4. Error growth involving more than one variable

a. Idealized weighting functions

Since many variables can influence errors in the forecasts of SST, a practical question arises: which variables must be determined most accurately at forecast initialization time to minimize SST forecast errors? Moore and Kleeman (1996) studied the energetics of error growth in their coupled model using an energy norm and found that thermocline data was more important than SST data for SST prediction. Xue et al (1997a), using a norm based on individual gridpoint variances, also concluded that thermocline information has more influence on the evolution of the system than initial SST information. Combining contributions from different variables is, however, inevitably somewhat arbitrary, since it depends on the definition of error and also on our understanding of where and in what variables the initial uncertainties are located.

The motivation here is to study how the features of the singular vectors depend on how we combine contributions from different variables. For simplicity, we confine attention to SST (**T**) and thermocline depth (**H**). In terms of a state vector represented by (**T**, **H**), the linear propagator can be expressed as

$$\mathbf{L} = \begin{pmatrix} \mathbf{L}_{TT} & \mathbf{L}_{HT} \\ \mathbf{L}_{TH} & \mathbf{L}_{HH} \end{pmatrix}, \tag{10}$$

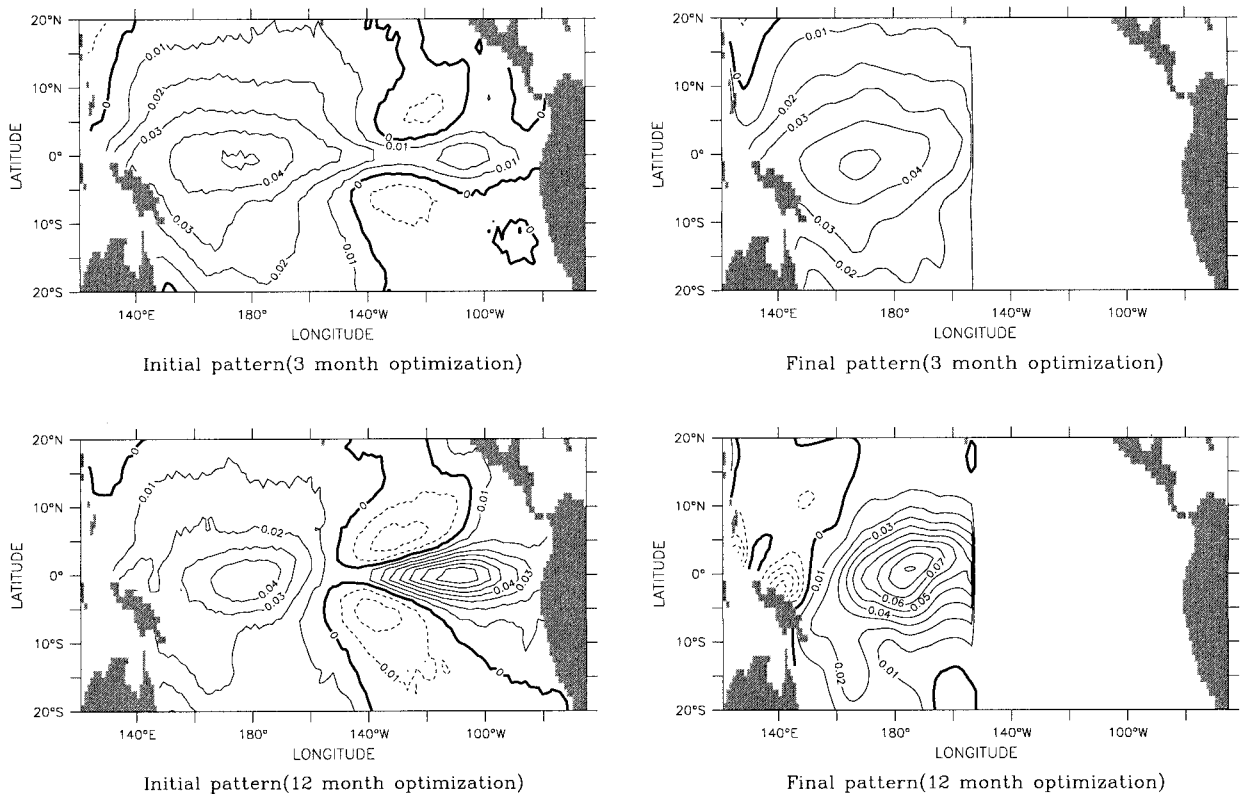

FIG. 2. As in Fig. 1, except that in the forecast norm zero weight is given to the eastern Pacific. Note the similarity between the 12-month initial singular vector in Figs. 1 and 2.

where $\mathbf{L}_{TT}$, $\mathbf{L}_{HT}$, $\mathbf{L}_{TH}$, and $\mathbf{L}_{HH}$ are the relevant linear propagators corresponding to different error growth processes. The propagator $\mathbf{L}_{TH}$ translates an initial error in $\mathbf{T}$ into a final error in $\mathbf{H}$, etc.

Initially, we assume uniform errors of magnitude σ_T^2 and σ_H^2 in $\mathbf{T}$ and $\mathbf{H}$, respectively:

$$\mathbf{P}_A = \mathbf{P}_F = \begin{pmatrix} 1/\sigma_T & & & \\ & \ddots & & \\ & & 1/\sigma_H & \\ & & & \ddots \end{pmatrix}. \quad (11)$$

According to Eq. (9), we have

$$\tilde{\mathbf{L}} = \mathbf{P}_F \mathbf{L} \mathbf{P}_A^{-1} = \begin{bmatrix} \mathbf{L}_{TT} & (\sigma_H/\sigma_T)\mathbf{L}_{HT} \\ (\sigma_T/\sigma_H)\mathbf{L}_{TH} & \mathbf{L}_{HH} \end{bmatrix}. \quad (12)$$

From Eq. (12), we can see that the dominant error growth, and therefore the singular vectors and singular values, depend crucially on the relative magnitude of σ_T and σ_H as also noted by Thompson (1998). For example, if we assume a typical uncertainty in SST $\sigma_T = 0.1$°C and in thermocline depth $\sigma_H = 10$ m, Fig. 3 shows that the dominant error growth process in this ''mixed norm'' is $\mathbf{H} \rightarrow \mathbf{T}$, suggesting that almost all of the initial information for the future development of the SST anomalies is contained within the initial ocean thermocline field. The results are similar for different optimization times and initialization dates. These results are similar to those of Moore and Kleeman (1996), who use an energy norm. In contrast, if we use $\sigma_T = 1.0$°C and $\sigma_H = 1$ m, the dominant error growth process is from $\mathbf{T} \rightarrow \mathbf{H}$ (not shown), implying that the initial errors in the thermocline field $\mathbf{H}$ are not important, and all useful information for future development of $\mathbf{H}$ anomalies is contained within the initial SST fields. In order to establish which error growth processes matter for real forecast errors, we need information about the size and spatial distribution of realistic initial errors.

b. Weighting based on a simulated analysis error covariance

The above results show that singular vectors are sensitive to the method used to weight initial and forecast errors. We now wish to investigate which are the best norms to use in calculating the singular vectors for initialization of ensemble forecasts.

The ideal analysis norm, $\mathbf{W}_A$, should reflect analysis uncertainty. The ideal forecast norm is more ambiguous, because it depends on the relative weight ascribed to forecast errors in different regions as discussed in sec-

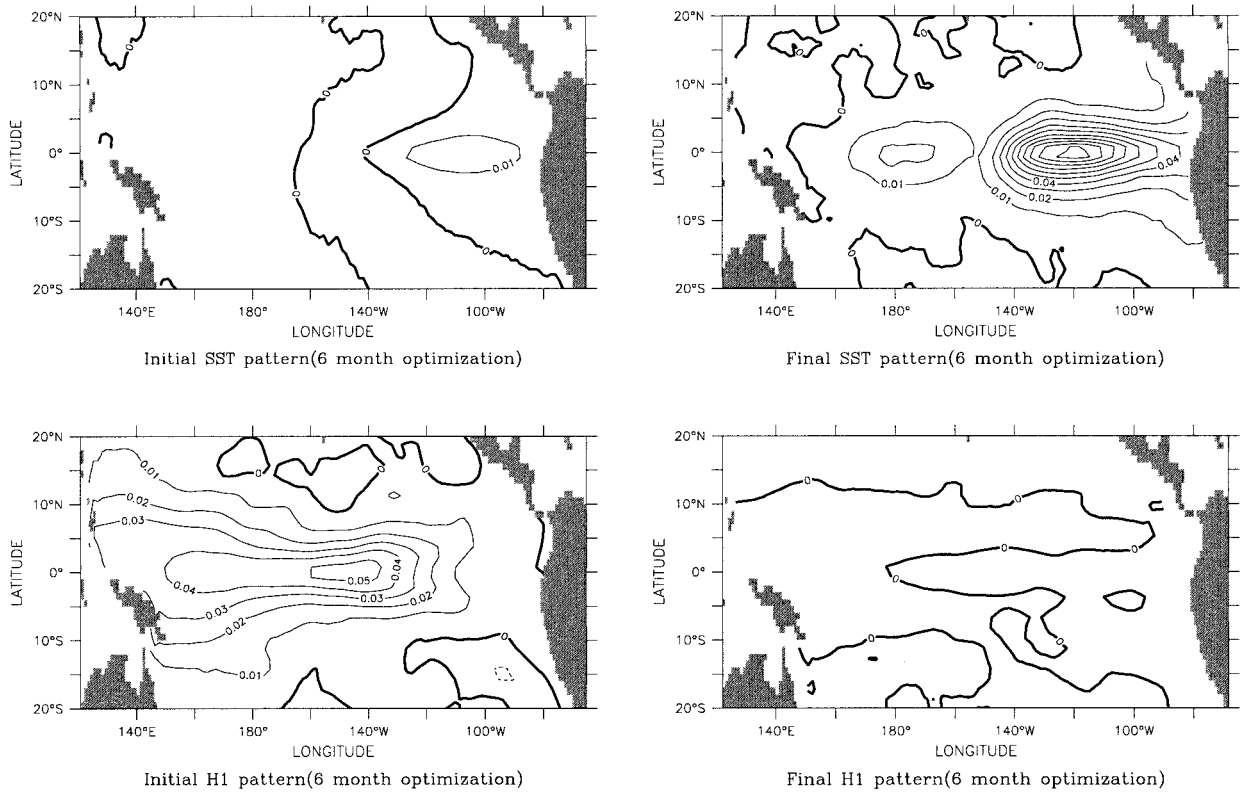

FIG. 3. Singular vectors using a mixed norm with $\sigma_T = 0.1$°C and $\sigma_H = 10$ m for a 6-month forecast initialized in Jan 1982. The relative magnitude of the different components indicates the dominant error growth process, in this case initial errors in **H** leading to final errors in **T**. The singular vectors are normalized in spectral (EOF) space, but displayed in physical space as defined in section 2b.

tion 3. However, the interpretation of error growth and singular values becomes complicated if different norms are used for analysis and forecast, so to simplify interpretation we use the same norm for both.

1) FEATURES OF SIMULATED ANALYSIS ERROR VARIANCES

In a real forecast situation it is difficult to know exactly the distribution of initial uncertainty. In this study, we estimate initial uncertainty in SST from the statistics of the difference between SST observations and a model simulation forced with observed winds, after the mean bias has been removed. If the model and SST observations were perfect, and therefore the only source of analysis and forecast error were errors in the forcing fields used for initialization (i.e., in our analysis procedure), this estimate would be accurate given a sufficiently long forced integration and observational record. In reality, of course, the model is imperfect, but this still provides a reasonable starting point.

We estimate **H** uncertainties from the difference of two model integrations with different wind forcing (see appendix B). This is less easy to justify, but in the absence of a long record of thermocline depth observations, we have little alternative. Recalling that, in an imperfect model, the analysis norm should reflect the statistics of the difference between the analysis and the corresponding point on the unknown shadowing trajectory, which yields the most accurate possible forecast in a given situation, basing this norm on the comparison of two trajectories seems reasonable, but it should be stressed that a more quantitative analysis of thermocline depth errors under different initialization schemes would be very useful.

Some insight into the characteristics of the simulated analysis SST (**T**) and **H** error covariance matrices can be obtained from their diagonal components, which represent error variance at a particular location. For ease of interpretation, we display rms values in Fig. 4. Figure 4 shows that estimated SST errors are mainly distributed between the central equatorial Pacific and the South American coast, in a pattern that is similar to the first EOF of SST.

The simulated analysis errors in **H** are mainly distributed between the central and western tropical Pacific. Since the wind fields used in the two model simulations to calculate errors in **H** are similar far from the equator, we underestimate the uncertainty in **H** there. As we are

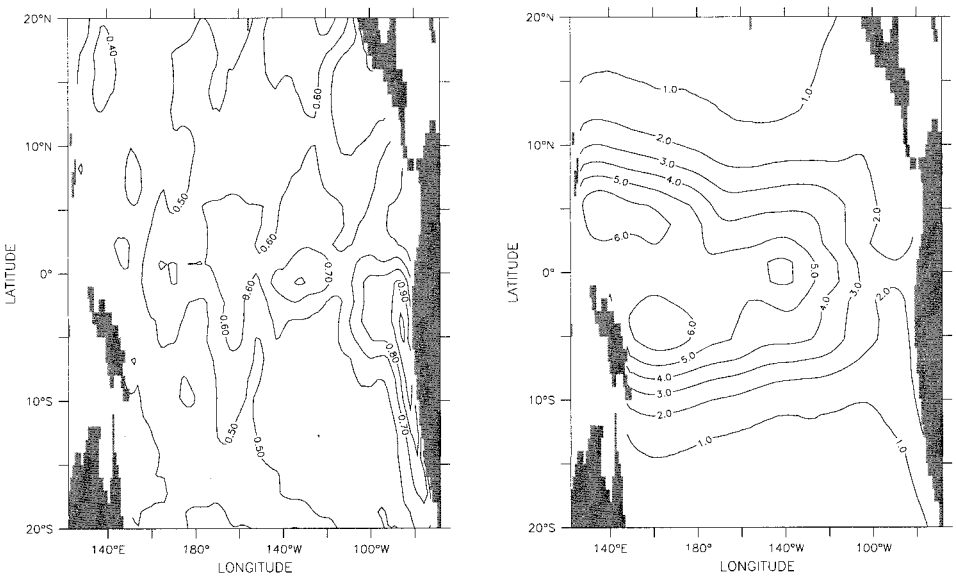

FIG. 4. Estimated rms analysis errors in SST (left, degrees) and thermocline depth (right, meters).

focusing on equatorial processes, this is not thought to be a major problem.

2) INFLUENCE OF SIMULATED ANALYSIS ERROR NORMS ON SINGULAR VECTORS

Singular vectors based on this estimated analysis norm for two different initialization dates are shown in Figs. 5 and 6. Both SST and **H** components of the initial and final singular vectors in Fig. 5 are of comparable magnitude, indicating that, on this occasion, there is no dominant error growth process in this coupled model when the the initial and final errors are constrained with simulated analysis error covariance matrices. These results indicate that initial uncertainty in both SST and **H** fields were equally important for predicting SST anom-

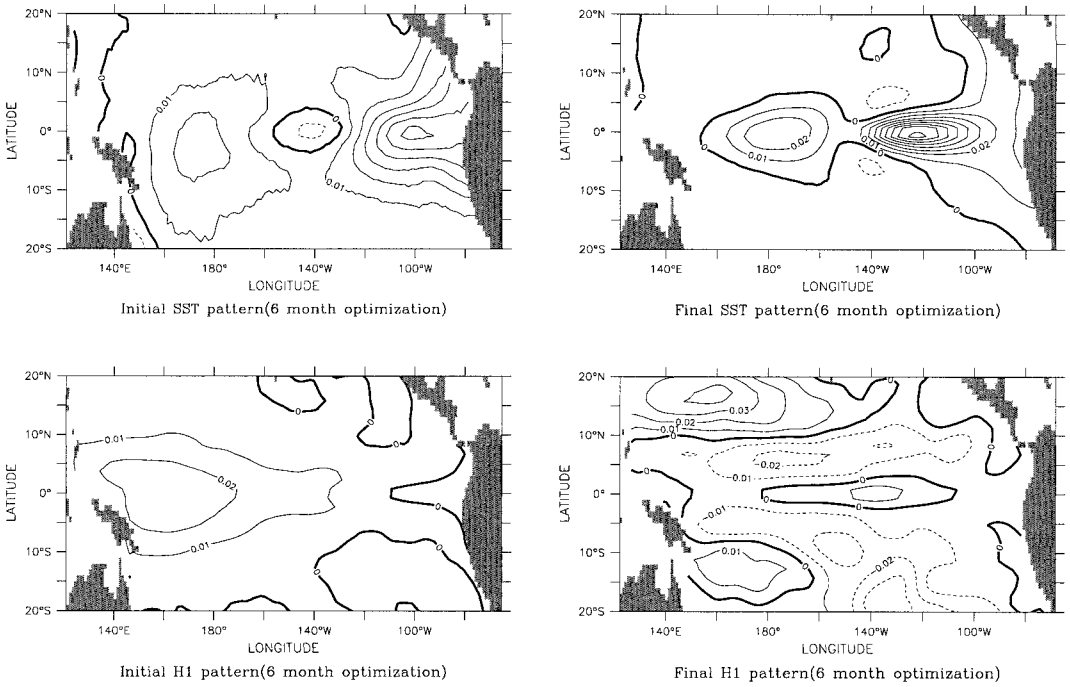

FIG. 5. Singular vectors under the mixed norm, optimization started in Jan 1982. The relevant first singular value is 6.32. Initial and forecast errors were weighted by the simulated analysis error covariance.

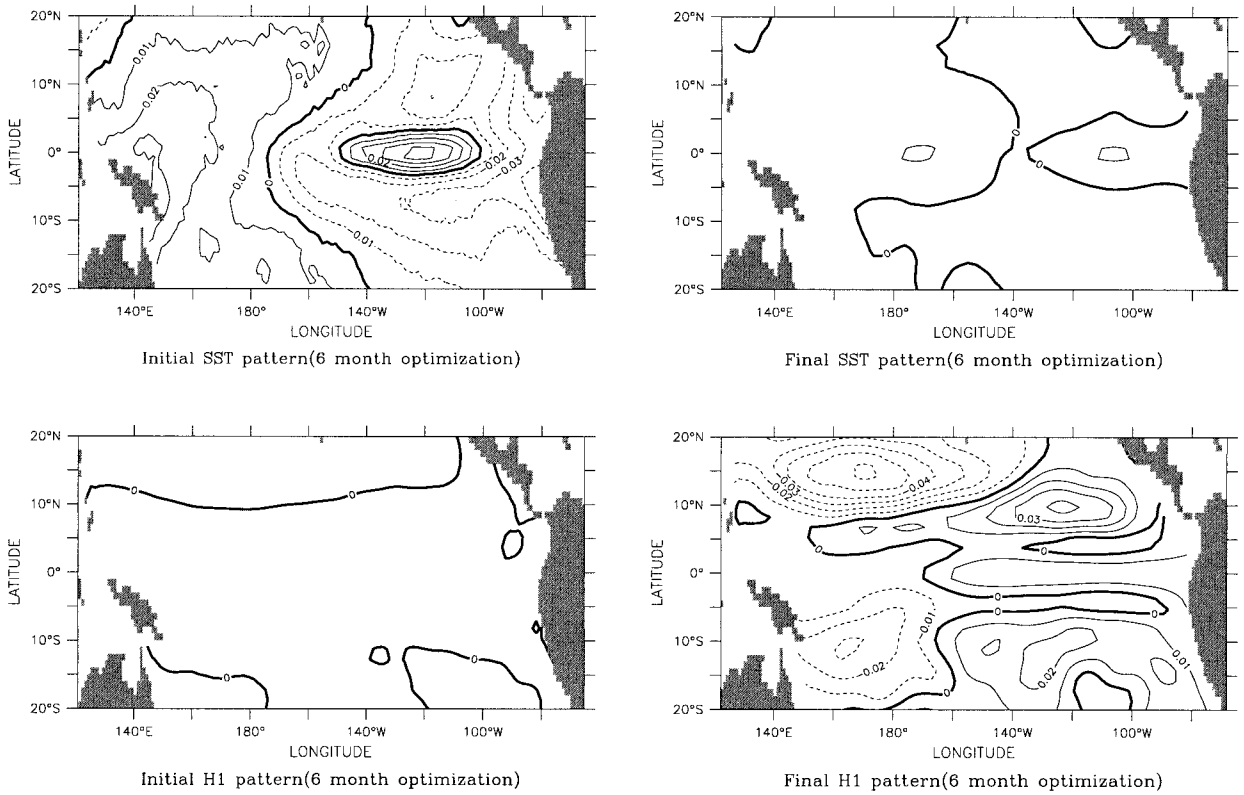

FIG. 6. Same as in Fig. 5 but optimization started in Jul 1982. The relevant first singular value is 6.25.

alies in the tropical Pacific at this time, in contrast to results obtained using other norms (Moore and Kleeman 1996; Xue et al 1997a). Thompson (1998), in a similar study with a mixed norm, found that the optimal SST pattern with a 0.1° anomaly produces the same size ENSO as the **H** pattern with 1.2-m thermocline anomaly.

Singular vectors from an optimization started 6 months later are shown in Fig. 6. In contrast to Fig. 5, initial errors in the SST field were evidently more important during this later period (July–December 1982), dominating error growth in the SST and **H** fields, and indicating that the singular vectors in the coupled model vary with initialization time.

The quantities plotted in Figs. 5 and 6 represent the singular vectors of the weighted linear propagator, $\tilde{\mathbf{L}}$, with the weighting given by the analysis norm [see Eq. (9)]. As such, some of the structure in these patterns will reflect the structure of the norm as well as the properties of the linear propagator itself. If we ignore the effect of EOF filtering, we can think of these initial patterns being operated on first by $\mathbf{P}_A^{-1}$ (which, in a diagonal analysis norm, would simply represent a weighting by the local analysis standard deviation) and then by the linearized model, $\mathbf{L}$, to give these final patterns. The final patterns would then themselves be weighted by $\mathbf{P}_F^T$ before calculating their size. If $\mathbf{L}$ were simply the unit matrix, the initial patterns would tend to be larger where the analysis errors are large. This makes sense in physical terms: if the dynamics do nothing to the errors, then the regions and variables in which we should be most concerned about initial errors are those in which the initial errors are likely to be largest, just as we should be most concerned about final errors in those regions and variables in which we would like forecast errors to be small.

From July 1982 to January 1983, the dominant errors appear to originate in SST, meaning that a small SST error (defined relative to the average size of SST analysis errors) would grow into a larger error in both SST and **H** than would an error in **H**, similiarly defined relative to the average size of **H** errors, over this period. This seems plausible, since by July 1982 the subsurface El Niño signal was already reasonably well established, whereas explosive growth of coupled SST/wind stress anomalies occurred primarily in the second part of that year; hence, the increase in the relative importance of SST errors between the earlier and later periods is considered.

Any growth of errors from an initial SST perturbation is likely to involve atmosphere–ocean coupling in this model, since the direct influence of SST on **H**, via nonlinearities in the ocean model thermodynamics, is relatively weak. Inspection of an animation of these singular vectors confirms that coupled processes (specifi-

cally the ''classic'' ENSO mechanism of anomalous zonal SST gradients in the central Pacific inducing a local zonal windstress anomaly that in turn enhances the SST gradient anomaly) do indeed play a dominant role in the evolution of errors originating in SST.

Errors in **H** can affect the other variables in the model more directly, but at lead times longer than 3 months or so, coupled processes also play an important role. The **H** anomalies in the western Pacific are a characteristic feature of many of the **H** initial singular vectors we have observed so far. The typical evolution observed in an animation is for these to propagate as equatorially trapped Kelvin waves into the central Pacific where they are amplified significantly by this coupled instability.

The results of this section indicate that the singular vectors are sensitive to the background error covariance matrices. Using the inverse of the simulated analysis error covariance as the error norm can influence the properties of optimal initial and final (SST and thermocline **H**) patterns and their growth rates significantly. This suggests that a reduction of analysis uncertainty in certain areas (particularly the eastern Pacific for SST and western Pacific for **H**, although this could be specific to this model and these particular initial conditions), then we might substantially improve the predictability of the coupled system.

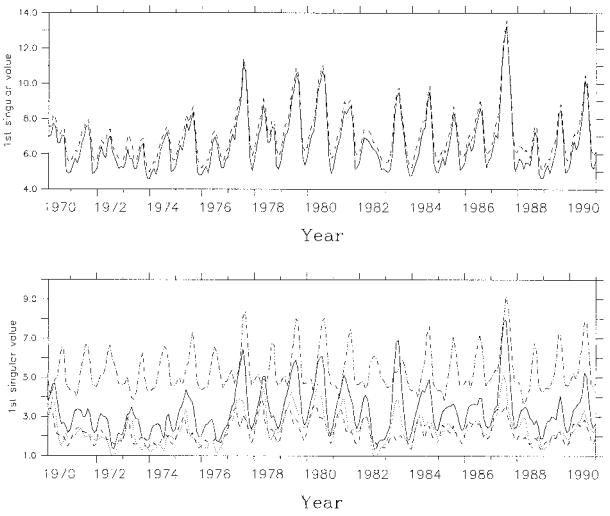

FIG. 7. First singular values (6-month optimization) from analysis errors and forecast errors weighted by simulated analysis error covariance matrices. (top) First singular values of the full linear propagator (solid line) and from root of sum of squared singular values of individual subpropagators (dashed line). (bottom) First singular values of individual subpropagators corresponding to different error growth processes. Solid line: **TT**, dashed line: **HH**, dotted line: **HT**, dot–dashed line: **TH**.

5. Temporal variability of error growth processes

In order to compare the relative importance of different error growth processes at different times, it is helpful to decompose the linear propagator into components relevant to the different processes. We can write the linear propagator $\mathbf{L}$, corresponding to error growth in both **T** and **H** in terms of the linear propagators corresponding to error growth in the individual variables [Eq. (10)], $\mathbf{L}_{TT}$, $\mathbf{L}_{HT}$, $\mathbf{L}_{TH}$, and $\mathbf{L}_{HH}$. The variance information of $\mathbf{L}$ is given by the sum of squares of its singular values:

$$\text{var}(\mathbf{L}) = \text{tr}(\mathbf{L}\mathbf{L}^{\text{T}}) = \sum_{i=1}^{r} \lambda_i^2, \tag{13}$$

where λ_i is ith singular value of $\mathbf{L}$, tr is trace operator, and r is the rank of the diagonal (singular values) matrix. From (10) we have

$$\mathbf{L}\mathbf{L}^{\text{T}} = \begin{pmatrix} \mathbf{L}_{TT}\mathbf{L}_{TT}^{\text{T}} + \mathbf{L}_{TT}\mathbf{L}_{HT}^{\text{T}} & \mathbf{L}_{TT}\mathbf{L}_{TH}^{\text{T}} + \mathbf{L}_{HT}\mathbf{L}_{HH} \\ \mathbf{L}_{TH}\mathbf{L}_{TT}^{\text{T}} + \mathbf{L}_{HH}\mathbf{L}_{HT}^{\text{T}} & \mathbf{L}_{TH}\mathbf{L}_{TH}^{\text{T}} + \mathbf{L}_{HH}\mathbf{L}_{HH}^{\text{T}} \end{pmatrix} \tag{14}$$

and therefore

$$\sum_i \lambda_i^2 = \sum_i \lambda_{TTi}^2 + \sum_i \lambda_{HTi}^2 + \sum_i \lambda_{THi}^2 + \sum_i \lambda_{HHi}^2. \tag{15}$$

If the first singular values dominate error growth in the coupled model, then we have

$$\lambda_1^2 \approx \lambda_{TT1}^2 + \lambda_{HT1}^2 + \lambda_{TH1}^2 + \lambda_{HH1}^2. \tag{16}$$

So the relative importance of different error growth processes at different times can be quantified by examining their contribution to λ_1^2.

Throughout this section we use the estimated analysis norm described in the previous section. Given the relative arbitrariness of this estimate, terms that depend on the assumed relative magnitude of SST and **H** errors (λ_{HT}^2 and λ_{TH}^2) should be interpreted with caution. We stress, however, that the same arbitrariness would apply to any assumed mixed norm encompassing both variables, and the use of this estimate at least ensures that these relative magnitudes are commensurate, at some level, with possible analysis errors. Similar results are obtained using a uniform mixed norm with $\sigma_T = 0.2$°C and $\sigma_H = 2.8$ m (Fan 1998).

a. Seasonal and interannual variation in singular values

The evolution of singular values obtained from individual and full optimizations during the 1970s and 1980s are shown in Fig. 7, for 6-month optimization times. The upper panel compares λ_1^2 from the full **T** and **H** propagators with the sum of the individual λ_{S1}^2, showing that the approximation in Eq. (16) is well satisfied. Hence we can use the relative size of λ_{TT1}, λ_{HT1}, λ_{TH1}, and λ_{HH1} to evaluate the relative importance of the corresponding ''subpropagators.'' Thompson (1998) obtained similar results.

The first point to note from the lower panel of Fig. 7 is that, for a 6-month optimization time, errors originating in SST seem to dominate error growth under

this norm (λ_{TH1} and λ_{TT1} are consistently greater than λ_{HT1} and λ_{HH1}), but all four processes are of comparable importance (none of the quantities displayed has a different order of magnitude from the others, as would happen if we were to use an energy norm). The importance of errors originating in SST could be exaggerated if we have underestimated terms involving **H** in our estimated analysis error covariance, but not by an order of magnitude. For a 12-month optimization time (not shown), development of SST errors into **H** errors (the $\mathbf{T} \rightarrow \mathbf{H}$ process, indicated by λ_{TH1}) still dominates predictability, but the other three error growth processes are now of roughly equal importance. We would argue that this suggests that reducing initialization errors in both SST and **H** are of comparable importance in improving ENSO prediction skill.

Focusing on λ_{TT1} and λ_{TH1}, interannual variability in total predictability seems to be dominated by processes resulting in SST errors, and is evidently closely related to ENSO (peaks in λ_{TT1} coincide with El Niño events). This may be interpreted physically, in that errors in SST are likely to grow fastest when the background SST anomalies are also developing rapidly at the onset of an El Niño event.

In contrast, the seasonal cycle in total predictability seems to be dominated by processes resulting in **H** errors (λ_{TH1}). Again, this makes sense in terms of the coupled model used. There is a strong seasonal cycle in thermocline depth as well as strong nonlinearity in the processes controlling **H** anomalies in the model ocean, so error growth is heavily dependent on how fast **H** anomalies *can* develop given the model background state at a particular point in the seasonal cycle. For a 12-month optimization time, error growth in **H** fields also shows clear interannual variability (not shown), as would be expected since coupled instabilities dominate errors at long lead times.

It is interesting to note that a singular value of the full propagator could be greater than unity (indicating growth) even when all of its constituent singular values from the subpropagators are less than unity (indicating decay). If two or more decaying singular vectors resulted from different processes project strongly onto each other, then they can still generate a growing mode in the coupled system—see, for example, Penland and Sardeshmukh (1995). The second singular values of the individual subpropagators ($\mathbf{L}_{TT}$, $\mathbf{L}_{HT}$, $\mathbf{L}_{TH}$, and $\mathbf{L}_{HH}$) are consistently smaller than 1.0, but the second singular values obtained from the corresponding full optimization indicate growth throughout the last two decades.

This result suggests that, if we restrict attention to only a single variable in our definition of error, we find only a single growing mode in this model; error growth is dominated by the first singular value. If, however, we consider interactions between different variables, then the first singular vector is no longer the only growing pattern; in most cases the second singular vector also grows.

b. Seasonal and interannual variations in singular vectors

Figure 8 shows the evolution of the equatorial component of the first initial and final singular vector, with the final singular vector multiplied by the corresponding singular value. The optimizations here are based on the simulated SST analysis error covariance matrices at the initial time and final time.

Some interesting properties emerge. First, the seasonal cycle dominates the evolution of the initial SST error patterns. Second, the optimal final SST errors not only vary with the seasonal cycle but also display clear interannual variability, which is closely associated with the ENSO events: during warm events the region of maximum growth seems to be the eastern Pacific, while during the cold episodes the growth of the errors is larger in the central Pacific.

We also examined the variability of the optimal **H** errors and found that the seasonal cycle is the dominant feature in both the optimal initial and final **H** errors.

c. Origins of seasonality in singular values

Singular values clearly vary with the seasonal cycle, raising the question of whether this seasonality results from seasonality in the strength of coupled instabilities (the so-called spring predictability barrier; Webster and Yang 1992) or simply from seasonality in the variance of anomalies in the variables under consideration (large SST anomalies, of either sign, only occur at certain times of year).

To explore this issue, we weighted every grid point with the inverse monthly standard deviation of SST anomalies in the Niño-3 region, thereby eliminating the seasonal cycle in Niño-3 anomaly variance, giving equal weight to average-sized anomalies in each season. To cross-check, we also multiplied by the standard deviation, to exaggerate the seasonal cycle artificially.

Figure 9 shows the seasonal cycle in the first singular value, averaged from 1970 to 1990, after the data have been preprocessed in this way. Weighting by the inverse monthly standard deviation of Niño-3 SST anomalies virtually eliminates the seasonal cycle in λ_{TT1}, indicating that much of the ''spring predictability barrier'' in this model results from seasonality in the variance of anomalies. The choice of the Niño-3 region to define the normalization does not appear to be critical—similar results are obtained weighting by local standard deviation.

6. Conclusions and discussion

Errors in the initial conditions of any coupled system are inevitable. In order to understand how predictability depends on the geographical location of the initial uncertainty and on the geographical location of accepted forecast errors, we have developed a simple and efficient

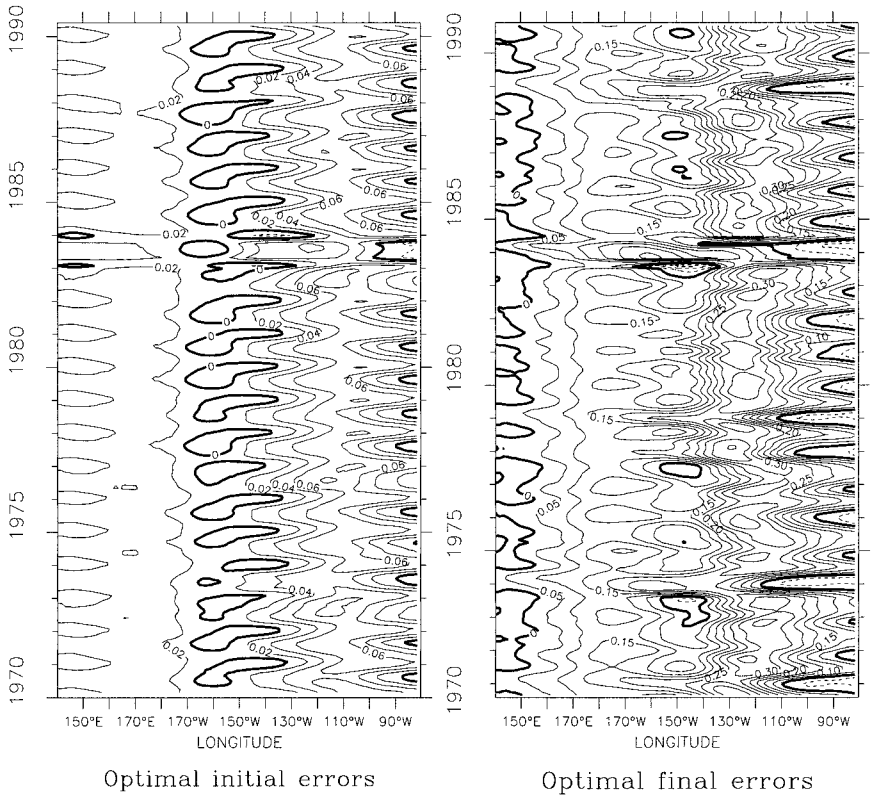

FIG. 8. Evolution of the optimal initial SST errors: (optimal initial patterns) and the optimal final SST errors: (optimal final patterns) × (first singular values) along the equator with 6-month optimization times.

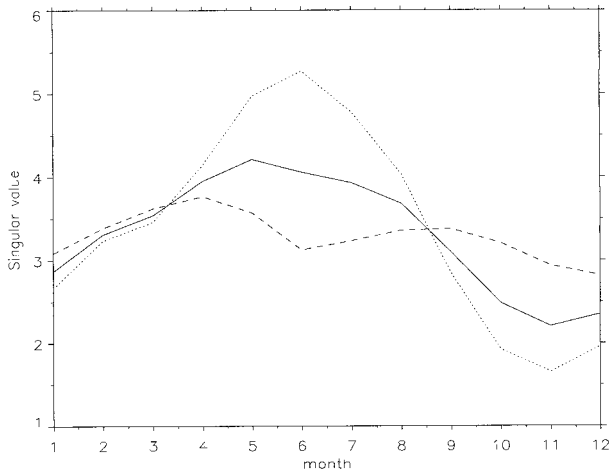

FIG. 9. Evolution of largest singular values (at the initial times) with 6-month optimization, averaged from 1970 to 1990. (a) Solid line: the initial and final errors are weighted by simulated analysis error covariance (SST norm); (b) dotted line: same as (a), but using seasonal Niño-3 SST rms errors (normalized) as weights; (c) dashed line: same as (a) but using inverse seasonal Niño-3 SST rms errors (normalized) as weights.

singular vector analysis technique that was used to explore the predictability of a coupled model for El Niño–Southern Oscillation (ENSO). The above method has proved very efficient in an intermediate coupled model; its extension to more comprehensive global (coupled) GCMs seems feasible.

Considering errors in the SST only, then, we find that to predict SST anomalies in the whole tropical Pacific 12 months ahead, the important initial SST information is located mainly in the eastern Pacific, whereas to predict SST anomalies in the western Pacific at 3-month lead times, the initial SST information is located mainly in the western Pacific itself.

We have to worry not just about errors in SST but also about errors in the subsurface thermal structure, represented in this model by the depth of the thermocline. As there is no unique way of combining information from two different variables, we have suggested one method, namely, the use of the analysis error covariance matrix, which seems a logical choice in the context of using singular vectors for forecasting. The difficulty is in accurately estimating this matrix. Our estimate is undoubtedly too crude and should be refined. Using the simulated analysis error covariance matrix as the norm to calculate the singular vectors, the results suggest that the initial information of both the SST field

and the thermocline field are important for SST prediction in the tropical Pacific. This is in contrast to the results using other norms, such as the energy norm (Moore and Kleeman 1996), which suggest that only thermocline information is important. If SST information is as important for ENSO predictions as our results suggest, then assimilating observed SST into forecast models may also be important for improving ENSO prediction. Intermediate models, such as this one or Zebiak and Cane, do not use SST information directly. However, other models, such as Stockdale et al. 1998 and Ji et al. 1998, give considerable weight to SST information.

Obviously, errors in SST forecasts can come from different sources, such as errors in the initial SST fields or in the initial ocean thermocline $\mathbf{H}$ fields or from model error. Understanding the relative importance of different initial error growth processes in the coupled system is important in developing a prediction model. A simple Eq. (16) can be used to quantify the relative importance of different error growth processes in the coupled model. The variability of the singular values and singular vectors of the coupled model in the 1970s and 1980s is explored. It reveals that both the singular values and final singular vectors not only vary with seasonal cycle but also show clear interannual variability, which is closely associated with ENSO events. So any initial errors in the SST and ocean thermocline fields, which project well onto the optimal initial patterns, may potentially induce or cancel an ENSO event and lead to a failed forecast.

The seasonality of singular values was also explored to some extent. The results suggest that the seasonality of singular values is at least partly related to the seasonal cycle in the variance in the predicted variables. Although some results here may be model specific, they may have some implications for other models.

Acknowledgments. The authors would like to thank the two anonymous reviewers and editor, James Hack, for their helpful comments and suggestions for improving the manuscript.

APPENDIX A

Estimation of the Linear Propagator

Rather than constructing the linear tangent model of the original model, we use a similar method to that suggested by Lorenz in 1965 to obtain the linear propagator directly from the full coupled model. The main difference is that we perturb the reference trajectory using a limited number of EOFs, giving a more efficient method of constructing the propagator. The procedure is as follows.

a. Control run

We select an initial condition in a particular time period of interest and run the coupled model from initial time t to some later time $t + \tau$, say, 1 yr, saving the intermediate (every 3 months) as well as final outputs from this control run as the ''reference trajectory.'' This control integration represents the model trajectory about which we will perform the approximate linearization.

b. Use selected EOF patterns either from model fields or from observed fields as initial perturbations to obtain the approximate tangent linear propagator $\mathbf{L}'$

The above integration is repeated, but using each of the obtained n EOF patterns (e.g., one of the first 50 EOFs) to perturb the selected initial oceanic state vector at the initial time t. The control integration is then subtracted from the perturbed model response at time $t + \tau$ (for some τ, chosen to be 3, 6, 9, and 12 months below) to obtain the final perturbation $\mathbf{r}'_i = (r'_{1i}, \ldots, r'_{mi})^{\mathrm{T}}$ at time $t + \tau$. Here i ($1 \le i \le n$) represents the ith EOF pattern and m represents the number of grid points of the perturbed state vector:

$$\begin{pmatrix} r'_{1i} \\ \vdots \\ r'_{mi} \end{pmatrix} = \mathbf{L} \begin{pmatrix} e_{1i} \\ \vdots \\ e_{mi} \end{pmatrix} \alpha'_i, \tag{A1}$$

where $\mathbf{e}_i = (e_{1i}, \ldots, e_{mi})^{\mathrm{T}}$ is the ith EOF pattern which is normalized, α'_i is the size of the ith EOF perturbation.

Repeating the above process using each selected EOF pattern in turn, we can build the approximation to the linear propagator ($\mathbf{L}'$). For n EOFs, Eq. (A1) in matrix form appears as

$$\begin{pmatrix} r'_{11} & \cdots & r'_{1n} \\ \vdots & \ddots & \vdots \\ r'_{m1} & \cdots & r'_{mn} \end{pmatrix} = \mathbf{L} \begin{pmatrix} e_{11} & \cdots & e_{1n} \\ \vdots & \ddots & \vdots \\ e_{m1} & \cdots & e_{mn} \end{pmatrix} \begin{pmatrix} \alpha'_1 & 0 & 0 \\ 0 & \ddots & 0 \\ 0 & 0 & \alpha'_n \end{pmatrix}. \tag{A2}$$

If we define $\mathbf{L}'$ as

$$\mathbf{L}' = \begin{pmatrix} r'_{11} & \cdots & r'_{1n} \\ \vdots & \ddots & \vdots \\ r'_{m1} & \cdots & r'_{mn} \end{pmatrix} \begin{pmatrix} \alpha'^{-1}_1 & 0 & 0 \\ 0 & \ddots & 0 \\ 0 & 0 & \alpha'^{-1}_n \end{pmatrix}, \tag{A3}$$

then the α' cancel out, and

$$\mathbf{L}' = \mathbf{L}\mathbf{E}, \tag{A4}$$

where $\mathbf{E}$ (where $\mathbf{E}^{\mathrm{T}}\mathbf{E} = \mathbf{I}_n$) is the matrix of selected EOF patterns that are used as basic perturbation fields. Here $\mathbf{L}$ is a $m \times m$ square matrix and $\mathbf{L}'$ is a $m \times n$ rectangular matrix. Note that Eq. (A4) is equivalent to Eq. (9) with $\mathbf{P}_F = \mathbf{I}$, $\mathbf{P}_A^{-1} = \mathbf{E}$, and $\hat{\mathbf{L}} = \mathbf{L}'$.

Postmultiplying both sides of Eq. (A4) by $\mathbf{E}^{\mathrm{T}}$ gives $\mathbf{L}\mathbf{E}\mathbf{E}^{\mathrm{T}} = \mathbf{L}'\mathbf{E}^{\mathrm{T}}$. If $\mathbf{E}$ consists of a complete set of EOFs (i.e., $m = n$), then $\mathbf{E}_m\mathbf{E}_m^{\mathrm{T}} = \mathbf{I}_m$ and

$$\mathbf{L} = \mathbf{L}'\mathbf{E}_m^T. \tag{A5}$$

In this case, exact singular vectors and singular values of $\mathbf{L}$ are obtained from the SVD of $\mathbf{L}'$, multiplying the

right singular vectors by $\mathbf{E}_m$ (see the definition of $\mathbf{R}_A$ in section 2b above). If, however, large parts of the initial errors can be explained by a small number of selected EOF patterns ($n \ll m$), then we can approximate $\mathbf{L}'$ with greater efficiency:

$$\mathbf{L} \cong \mathbf{L}'\mathbf{E}^{\mathrm{T}}_{n \ll m}. \tag{A6}$$

The results from the 1970s and 1980s indicate that we can obtain stable and consistent singular vectors using only 10 model EOF patterns. Therefore, if not mentioned, all the results in this paper are based on 10 model EOF patterns as the initial perturbations.

As stressed in the text, this procedure confines attention to large spatial scales, and therefore not all possible error growth processes will be captured by this analysis. We believe, however, that all processes that can realistically be simulated by this model are adequately represented.

APPENDIX B

Estimation of Analysis Error Covariance Matrices

The problem of estimation of the analysis error covariance matrices is twofold. On one hand, we need to estimate the ''physical'' properties (magnitude and spatial distribution) of the uncertainties in SST and **H** fields (estimation of $\mathbf{C}_A$). On the other hand, we need a mathematical formulation compatible with our reduced-rank linear propagator.

To estimate the uncertainties in SST we use the differences between observations of SST and a model simulation forced with observed FSU winds for the period 1961–91. As the model simulation does not include information of the observed SST, it may well be that we overestimate the magnitude of initial errors in SST for a typical state-of-the-art analysis system. However, this estimation is consistent with the initialization procedure used in this study.

There is no record of thermocline depth measurements that is long enough to allow estimation of the error distribution in the **H** field. Instead, uncertainties in the **H** field are computed using the differences between two model simulations forced with different wind fields: FSU winds and ''filtered'' FSU winds. The filtered winds are obtained by applying a linear filter to the interannual anomalies of the FSU, with the idea of removing undesirable noise. The linear filter is obtained using a statistical relationship between observed SST and FSU winds anomalies in such a way that only the information of the winds that is coherent with the SST evolution will be retained. This statistical filter is only applicable near the equator (where the SST and winds show stronger correlation). Outside the regions where the filter is active, the original winds are used. Therefore, differences between raw and filtered winds will be restricted to the equatorial band, and so will be our estimation of the uncertainty in the **H** field.

We obtain an estimate of the analysis error covariance matrix $\mathbf{C}_A$ in the original m-dimensional space simply by averaging over the ℓ available ''error patterns,'' thus:

$$\frac{1}{\ell}\mathbf{G}\mathbf{G}^{\mathrm{T}} = \hat{\mathbf{C}}_A(m, m) = \begin{pmatrix} \hat{\mathbf{C}}_{TT} & 0 \\ 0 & \hat{\mathbf{C}}_{HH} \end{pmatrix}, \tag{B1}$$

where the columns of $\mathbf{G}$, $\mathbf{g}_i = (\mathbf{T}'_i, \mathbf{H}'_i)$, consists of the ''SST error'' (control–observation difference) and the ''**H** error'' (raw-forcing minus filtered forcing) at time i.

We now introduce a method of estimating $\mathbf{P}_A$ and $\mathbf{P}_A^{-1}$ from our estimate of the analysis error covariance matrix taking into account the fact that $\hat{\mathbf{C}}_A$ is noninvertible. At this stage we already know $\mathbf{L}'$, which operates in a reduced space spanned by the first n EOFs $\mathbf{E}$ of the control run (as detailed in appendix A). The trick is to recognize that we do not actually require the full inverse of $\hat{\mathbf{C}}_A$ but only the pseudo-inverse in the subspace spanned by these n EOFs. That is, we require

$$\mathbf{P}_A^{\mathrm{T}}\mathbf{P}_A = \hat{\mathbf{C}}_A^{(-1)_n}. \tag{B2}$$

$\mathbf{P}_A$ can be obtained as follows.

1) Project the $\mathbf{G}$ onto the n leading EOF patterns $\mathbf{E}$ (first EOF space), which can also be used as the initial perturbations, and Eq. (B1) can be written as

$$\mathbf{E}^{\mathrm{T}}\left(\frac{1}{\ell}\mathbf{G}\mathbf{G}^{\mathrm{T}}\right)\mathbf{E} = \mathbf{C}'_A(n, n) = \mathbf{U}\mathbf{\Sigma}^2\mathbf{U}^{\mathrm{T}}(n, n), \tag{B3}$$

   where $\mathbf{U}$ is a new set of EOFs, representing the eigenvectors of the analysis error covariance matrix in the subspace defined by $\mathbf{E}$. The new set of EOFs is derived from $\mathbf{E}^{\mathrm{T}}\mathbf{G} = \mathbf{U}\mathbf{\Sigma}\mathbf{V}^{\mathrm{T}}$, with normalization $(1/\ell)\mathbf{V}^{\mathrm{T}}\mathbf{V} = \mathbf{I}$.

2) Further truncate, if necessary, and diagonalize $\mathbf{C}'$ by projection onto the first s elements of $\mathbf{U}$:

$$\mathbf{U}^{\mathrm{T}}\mathbf{E}^{\mathrm{T}}\left(\frac{1}{\ell}\mathbf{G}\mathbf{G}^{\mathrm{T}}\right)\mathbf{E}\mathbf{U} = \mathbf{\Sigma}^2(s, s). \tag{B4}$$

3) Estimate the truncated inverse analysis error covariance matrix $\hat{\mathbf{C}}_A^{(-1)_n}$, in the original m-dimensional space from

$$\begin{aligned}\hat{\mathbf{C}}_A^{(-1)_n} &= \mathbf{E}\mathbf{U}\left[\mathbf{U}^{\mathrm{T}}\mathbf{E}^{\mathrm{T}}\left(\frac{1}{\ell}\mathbf{G}\mathbf{G}^{\mathrm{T}}\right)^{-1}\mathbf{E}\mathbf{U}\right]\mathbf{U}^{\mathrm{T}}\mathbf{E}^{\mathrm{T}} \\ &= \mathbf{E}\mathbf{U}\mathbf{\Sigma}^{-2}\mathbf{U}^{\mathrm{T}}\mathbf{E}^{\mathrm{T}}.\end{aligned} \tag{B5}$$

4) Combining Eqs. (B5) with (B2) and (B3) we obtain the expression for the projectors:

$$\mathbf{P}_A = \mathbf{E}\mathbf{U}\mathbf{\Sigma}^{-1}\mathbf{U}^{\mathrm{T}}\mathbf{E}^{\mathrm{T}} \tag{B6}$$

$$\mathbf{P}_A^{-1} = \mathbf{E}\mathbf{U}\mathbf{\Sigma}\mathbf{U}^{\mathrm{T}}\mathbf{E}^{\mathrm{T}}. \tag{B7}$$

Thus, the maximization problem (8) reduces to an SVD of

$$\mathbf{P}_F\mathbf{L}\mathbf{P}_A^{-1} = \mathbf{P}_F\mathbf{L}\mathbf{E}\mathbf{U}\mathbf{\Sigma}\mathbf{U}^{\mathrm{T}}\mathbf{E}^{\mathrm{T}} \tag{B8}$$

$$= \mathbf{P}_F\mathbf{L}'\mathbf{U}\mathbf{\Sigma}\mathbf{U}^{\mathrm{T}}\mathbf{E}^{\mathrm{T}}, \tag{B9}$$

where $\mathbf{L}'(m, n)$ is our approximation to the tangent linear propagator, described in appendix A. Since $\mathbf{E}^{\mathrm{T}}$ is an orthonormal matrix, we only need to apply SVD to $\mathbf{P}_F\mathbf{L}'\mathbf{U}\mathbf{\Sigma}\mathbf{U}^{\mathrm{T}}$ whose dimension is (m, n).

We can also obtain the $\mathbf{P}_F$ using the above method. Thus, the maximum possible error growth can be represented by the largest (first) singular value of the propagator, $\mathbf{P}_F\mathbf{L}\mathbf{P}_A^{-1}$. The optimal initial and final patterns that accomplish this error growth are the right and left singular vectors of $\mathbf{P}_F\mathbf{L}\mathbf{P}_A^{-1}$.

REFERENCES

Anderson, D. L. T., and J. P. McCreary, 1985: Slowly propagating disturbances in a coupled ocean–atmosphere model. *J. Atmos. Sci.,* **42,** 615–629.

Balmaseda, M., D. L. T. Anderson, and M. K. Davey, 1994: ENSO prediction using a dynamical ocean model coupled to statistical atmospheres. *Tellus,* **46A,** 497–511.

Battisti, D. S., 1988: The dynamics and thermodynamics of a warming event in a coupled tropical atmosphere–ocean model. *J. Atmos. Sci.,* **45,** 2889–2919

Blumenthal, M. B., 1991: Predictability of a coupled ocean–atmosphere model. *J. Climate,* **4,** 766–784.

Chen, S. S., and R. A. Houze Jr., 1997: Interannual variability of deep convection over the tropical warm pool. *J. Geophys. Res.,* **102,** 25 783–25 795.

Chen, Y.-Q., D. S. Battisti, T. N. Palmer, J. Barsugli, and E. S. Sarachik, 1997: A study of the predictability of tropical Pacific SST in a coupled atmosphere–ocean model using singular vector analysis: The role of the annual cycle and the ENSO cycle. *Mon. Wea. Rev.,* **125,** 831–845.

Fan, Y., 1998: ENSO prediction and predictability in an intermediate coupled model. Ph.D. thesis, University of Oxford, 241 pp. [Available from Bodleian Library, University of Oxford, Broad St., Oxford OX1 3BG, United Kingdom.]

Gilmour, I., 1999: Nonlinear model evaluation: ι-shadowing, probabilistic prediction and weather forecasting. Ph.D. thesis, University of Oxford, 183 pp. [Available from Bodleian Library, University of Oxford, Broad St., Oxford OX1 3BG, United Kingdom.]

Goldberg, S. D., and J. J. O'Brien, 1981: Time and space variability of tropical Pacific wind stress. *Mon. Wea. Rev.,* **109,** 1190–1207.

Ji, M., D. Behringer, and A. Leetmaa, 1998: An improved coupled model for ENSO prediction and implications for ocean initialization. Part II: The coupled model. *Mon. Wea. Rev.,* **126,** 1022–1034.

Lorenz, E. N., 1965: A study of the predictability of a 28-variable atmospheric model. *Tellus,* **17,** 321–333.

McCreary, J. P., and D. L. T. Anderson, 1991: An overview of coupled ocean–atmosphere models of El Niño and Southern Oscillation. *J. Geophys. Res.,* **96,** 3125–3150.

Moore, A. M., and R. Kleeman, 1996: The dynamics of error growth and predictability in a coupled model of ENSO. *Quart. J. Roy. Meteor. Soc.,* **122,** 1405–1446.

——, and ——, 1997: The singular vectors of a coupled ocean–atmosphere model of ENSO. II: Sensitivity studies and dynamical interpretation. *Quart. J. Roy. Meteor. Soc.,* **123,** 983–1006.

Oberhuber, J. M., 1988: An atlas based on COADS dataset: The budgets of heat, buoyancy and turbulent kinetic energy at the surface of global ocean. Max-Planck-Institut für Meteorologie, Tech. Rep. 15, Hamburg Germany. [Available from Max-Planck-Institut für Meteorologie, Bundesstrasse 55, D-20146 Hamburg, Germany.]

Palmer, T. N., 1996: Predictability of the atmosphere and oceans: From days to decades. *Decadal Climate Variability-Dynamics and Predictability,* D. L. T. Anderson and J. Willebrand, Eds., NATO ASI Series, Vol. 44, Springer-Verlag, 83–155.

——, and D. A. Mansfield, 1984: Response of two atmospheric general circulation models to sea-surface temperature anomalies in the tropical East and West Pacific. *Nature,* **310,** 483–485.

Penland, C., and P. Sardeshmukh, 1995: The optimal growth of tropical sea surface temperature anomalies. *J. Climate,* **8,** 1999–2024.

Stockdale, T. N., D. L. T. Anderson, J. O. S. Alves, and M. A. Balmaseda, 1998: Global seasonal rainfall forecasts using a coupled ocean–atmosphere model. *Nature,* **392,** 370–373.

Thompson, C. J., 1998: Initial conditions for optimal growth in a coupled ocean–atmosphere model of ENSO. *J. Atmos. Sci.,* **55,** 537–557.

Webster, P. J., and S. Yang, 1992: Monsoon and ENSO: Selectively interactive systems. *Quart. J. Roy. Meteor. Soc.,* **118,** 877–926.

Xue, Y., M. A. Cane, S. E. Zebiak, and M. B. Blumenthal, 1994: On the prediction of ENSO—A study with a low-order Markov model. *Tellus,* **46A,** 512–528.

——, ——, and ——, 1997a: Predictability of a coupled model of ENSO using singular vector analysis. Part I: Optimal growth in seasonal background and ENSO cycles. *Mon. Wea. Rev.,* **125,** 2043–2056.

——, ——, and ——, 1997b: Predictability of a coupled model of ENSO using singular vector analysis. Part II: Optimal growth and forecast skill. *Mon. Wea. Rev.,* **125,** 2057–2073.

Zebiak, S. E., and M. A. Cane, 1987: A model El Niño–Southern Oscillation. *Mon. Wea. Rev.,* **115,** 2262–2278.